Evaluation of Cell Type Deconvolution R Packages on Single Cell RNA-seq Data

Qianhui Huang[1], Yu Liu[2], Yuheng Du[1], Lana X. Garmire[2 *]

[1] *Department of Biostatistics, University of Michigan, Ann Arbor, 48109, USA*

[2] *Department of Computational Medicine and Bioinformatics, University of Michigan, Ann Arbor, 48105, USA.*

* To whom correspondence should be addressed. Email address: lgarmire@med.umich.edu

Abstract

Annotating cell types is a critical step in single cell RNA-Seq (scRNA-Seq) data analysis. Some deconvolution methods have recently emerged to enable automated cell type identification. However, comprehensive evaluations of these methods are lacking to provide practical guidelines. Moreover, it is not clear whether some deconvolution methods originally designed for analyzing other omics data are adaptable to scRNA-Seq analysis. In this study, we evaluated ten cell-type deconvolution methods publicly available as R packages. Eight of them are popular methods developed specifically for single cell research (Seurat, scmap, SingleR, CHETAH, SingleCellNet, scID, Garnett, SCINA). The other two methods are repurposed from deconvoluting DNA methylation data: Linear Constrained Projection (CP) and Robust Partial Correlations (RPC). We conducted systematic comparisons on a wide variety of public scRNA-seq datasets as well as simulation data. We assessed the accuracy through intra-dataset and inter-dataset predictions, the robustness over practical challenges such as gene filtering and high similarity among cell types, as well as the capabilities on rare and unknown cell-type detection. Overall, methods such as Seurat, SingleR, CP, RPC and SingleCellNet performed well, with Seurat being the best at annotating major cell types. Also, Seurat, SingleR and CP are more robust against down-sampling. However, Seurat does have a major drawback at predicting rare cell populations, and it is suboptimal at differentiating cell types that are highly similar to each other, while SingleR and CP are much better in these aspects.

KEYWORDS: Single cell; Single cell RNA sequencing; scRNA-seq; cell type; annotation; classification; deconvolution; benchmark; simulation;

Introduction

Single cell RNA sequencing (scRNA-seq) has emerged as a powerful tool to enable the characterization of cell types and states in complex tissues and organisms at the single-cell level [1–5]. Annotating cell types amongst the cell clusters is a critical step before other downstream analyses, such as differential gene expression and pseudo time analysis [6][7][8][9]. Conventionally, a set of priorly known cell-type specific markers are used to label the cell types of the clusters manually. This process is laborious and often is a rate-limiting step for scRNA-seq analysis. This approach is also prone to bias and errors. The marker may not be specific enough to differentiate the cell subpopulations in the same dataset, or it may not be generic enough to be applied from one study to another. Automating the cell type labeling is critical to enhance reproducibility and consistency among single cell studies.

Recently some deconvolution methods have emerged to systematically assign cell types in the new scRNA-seq dataset, based on existing annotations from another dataset. Instead of using only top differentiating markers, most methods project or correlate the new cells onto similar cells in the well-annotated reference datasets, by leveraging the whole transcriptome profiles. These deconvolution methods are developed rapidly, at the same time benchmark datasets that the bioinformatics community agrees upon are lacking. These issues pose the urgent need to comprehensively evaluate these deconvolution methods using datasets with different biological variabilities, protocols and platforms. It is essential to provide practical guidelines for users. Additionally, identification of limitations of each method through comparisons will also help boost further algorithmic development, which in turn will benefit the scRNA-Seq community.

In this study, we evaluated ten cell deconvolution methods publicly available as R packages (**Table 1**). Eight of them are popular methods developed specifically for single cell research (Seurat [10], scmap [11], SingleR [12], CHETAH [13], SingleCellNet [14], scID [15], Garnett [16], SCINA [17]). Those methods can be further divided into two categories: Seurat, scmap, CHETAH, SingleCellNet, and scID utilize the gene expression profile as a reference without prior knowledge in signature sets, while Garnett and SCINA require additional pre-defined gene markers as the input. Additionally, to potentially leverage exiting deconvolution methods for other omics data, we also included two modified methods: Linear Constrained Projection (CP) and Robust Partial Correlations (RPC) that are popular in DNA methylation analysis [18]. We

conducted systematic comparisons on six publicly available scRNA-seq datasets (**Table 2**) varying by species, tissue and sequencing protocol, as well as six sets of simulation data with known truth measure.

Results

Intra-dataset accuracy evaluation

We first tested the deconvolution accuracy of 10 methods (**Table 1**) on six publicly available scRNA-seq datasets (**Table 2**). These datasets include two human pancreatic islet datasets (GSE85241 and GSE86469), two whole mouse datasets (Tabula Muris, or TM-Full), and two peripheral blood mononuclear cells datasets (PBMC). Since Tabula Muris datasets are heterogeneous in terms of tissue contents, to evaluate the tools' performance on homogeneous data, we down sampled them separately into two mouse lung datasets (Tabula Muris-Lung, or TM-Lung) by taking cells from lung tissue only. This results in eight real scRNA-seq datasets (**Table 1**). To avoid potential bias, we used the 5-fold cross validation scheme to measure the averaged accuracy in the 1-fold holdout subset. We used three different performance measurement metrics: overall accuracy, adjusted rand index (ARI), and V-measure [19] [20] (see **Methods**). The evaluation workflow is depicted in **Figure S1**.

Figure 1A-C show the classification accuracy metrics on eight datasets. The top-five performing deconvolution methods are Seurat, SingleR, CP, singleCellNet and RPC. Seurat has the best overall classification performance in the 5-fold cross validation evaluation. On average, the three accuracy metrics from Seurat are significantly higher (Wilcoxon paired rank test, $P<0.05$) than 9 other methods. SingleR has the second-best performance after Seurat, with all three metrics higher than 8 other methods, among which 6 pair-wise method comparisons achieved statistical significance (Wilcoxon paired rank test $P < 0.05$). Though slightly lower in average metric scores, the classification performance of both singleCellNet and CP are comparable to SingleR.

In order to test the influence of cell-type number on tool's performance, we next evaluated the TM-Full and TM-Lung results. As shown in **Table 2**, for two TM-Full datasets from 10X and Smart-Seq2 platforms, which contain a large number of cell types (32 and 37 cell types, respectively), we took a subset of cells from the lung tissue and created two TM-Lung datasets that are relatively small in cell-type numbers, with 8 and 10 cell types for 10X and Smart-Seq2

platforms, respectively. Most methods perform well for both TM-Lung datasets with ARI > 0.9. However, some of the methods had a drop of performance on the two TM-Full datasets. The increased classification labels imposed a challenge. Garnett failed to predict on such large TM-Full datasets. Additionally, SCINA, CHETAH and scmap have significantly lower classification metrics on TM-Full datasets, compared to those on TM-Lung datasets. On the contrary, the previously mentioned top-five methods are more robust despite the increase of complexity in TM-Full datasets. Again, Seurat yields the best metric scores in both TM-Full datasets, demonstrating its capability at analyzing complex datasets.

Cross-dataset accuracy evaluation

To evaluate the deconvolution tools in a more realistic setting, we conducted cross-dataset performance evaluation on 10 datasets (5 pairs), where the referencing labels were obtained from one dataset and the classification was done on another dataset of the same tissue type (**Table 2**). Within a pair, we used sorted, purified dataset as the reference data, and the remaining one as the query data (see **Methods**). Among the 5 pairs of datasets, 4 are real experimental data: PBMC cell pair with PBMC-sorted-ref and PBMC-3K-query; pancreas cell pair with pancreas-celseq2-ref and pancreas-fluidigm-query; TM-Full pair with TM-Full-smartseq2-ref and TM-Full-10X-query; TM-Lung pair with TM-Lung-smartseq2-ref and TM-Lung-10x-query. The last pair is simulation datasets with the pre-defined truth, where the true assay without dropouts (simulation_true-ref) was used as the reference and the raw assay with dropout mask (simulation_raw-query) was used as the query.

Figure 1D-F shows the classification accuracy metrics on the above mentioned 5 pairs of query and reference datasets. The top 3 performing deconvolution methods in the descending rank order are Seurat, SingleR, and CP, the same as those in the same-dataset cross validation results (**Figure 1A-C**). In particular, they all perform very well on the simulation data with known truth measures, as all three accuracy metrics are above 0.96. RPC is ranked 4th, slightly better than SCINA. Similar to the 5-fold cross validation evaluation, methods such as scID, CHETAH, scmap and Garnett are persistently ranked among the lowest-performing methods for accuracy. Interestingly, singleCellNet, the method that performs relatively well (ranked 4th) in the same-dataset 5-fold cross validation, is now consistently ranked on the 6th, behind RPC and SCINA, due to drop of performance in TM-Full datasets. Besides deconvolution methods, the accuracy scores are also

much dependent on the datasets. For example, on complex PBMC datasets, even Seurat only reaches 0.76 for ARI. A further examination of the confusion matrices (**Figure S3**) for Seurat, SingleR, CP, singleCellNet and RPC reveals that the challenge comes from distinguishing highly similar cell types such as CD4+ T cells vs. CD8+ T cells or Dendritic cells vs. CD14+ Monocytes in the PBMC datasets.

Altogether, these results from both experimental and simulation data indicate that Seurat has the best overall accuracy among the deconvolution methods in comparison, based on intra-dataset prediction and cross-dataset prediction [10].

The effect of cell type similarity on deconvolution performance

Since it is challenging to distinguish highly similar cell populations using cross-data evaluation, we next conducted simulations. We designed four simulation data sets composed of five cell groups with varying levels of differential expression. We used Splatter [21] to pre-define the same set of differential expression (DE) genes in the four simulation datasets, and only differed the magnitudes of DE, from low, low-moderate, moderate to high (**Figure 2A**). When cell populations are more separable, the classification task is easy for the majority of methods. As the cell populations become less separable, all methods show a decrease in their performance (**Figure 2B-D**). The degrees of such decrease vary among the methods though. SingleR, RPC, Seurat, singleCellNet and CP are in the first class that are relatively more robust than the other five methods. SingleR and RPC are ranked the 1st and 2nd for their robustness against cell type similarity, with all three metric scores above 0.9. Seurat is ranked the 4th after singleCelNet (the 3rd) when the samples are least separable, exposing its slight disadvantage.

The effect of gene filtering on deconvolution performance

We also evaluated the stability of deconvolution methods in inter-dataset classification, by varying the number of query input features. For this purpose, we used the human pancreas data pair (**Table 2**). We randomly down sampled the features from Fluidigm data into 15,000, 10,000 and 5,000 input genes, based on the original log count distribution (**Figure 3A**). When the number of features decreases, most methods show decreased metric scores as expected (**Figure 3B**). Seurat and SingleR are the top 2 most robust methods over the decrease of feature numbers, and their ARI scores remain high across all sampling sizes (ARI > 0.9). Again, methods such as Garnett, scID

and scmap are more susceptible to low feature numbers, since their performances decrease as the feature number decreases. Therefore, using query data with fewer features than the reference data may affect the prediction performance of those methods. Alternatively, we also downsized the samples by reducing the number of raw reads before alignment and tag counting steps (**Figure 3C**). While most methods show fairly consistent accuracy scores with reduced raw reads as expected, a couple of methods, such as singleCellNet and scID, are perturbed by this procedure (**Figure 3D**).

Evaluation of rare population detection

Identifying rare populations in single cells is a much biologically interesting aspect. We evaluated the inter-dataset classification accuracy per cell population for the top 5 methods: Seurat, SingleR, CP, singleCellNet and RPC (**Figure 1A-B**). We used a mixture of 9 cell populations with a wide variety of percentages (50%, 25%, 12.5%, 6.25%, 3.125%, 1.56%, 0.97%, 0.39%, 0.195%) in a simulation dataset (**Figure 4A**). When the size of the cell population is larger than 50 cells out of 2000 cells, all five methods achieve high cell-type specific accuracy of over 0.8 (**Figure 4B**). However, the classification performances drop drastically for Seurat and singleCellNet when the cell population is 50 or less. Interestingly, bulk-reference based methods such as SingleR, CP and RPC are extremely robust against the size changes of a cell population, revealing their advantages in classifying rare cell types.

Evaluation of unknown population(s) detection

Among the scRNA-seq specific deconvolution tools, five methods (Garnett, SCINA, scmap, CHETAH, scID) contain the rejection option that allows ‘unassigned’ labels. This is a rather practical option, as the reference data may not contain all cell labels present in the query data. In order to assess how accurate these methods are at labeling ‘unassigned’ cells, we used the scheme of “hold-out one cell type evaluation” on the same simulation dataset pair used in cross-dataset prediction. That is, we remove the signature of one cell type in the reference matrix while keeping the query intact. The evaluation repeated five times for all five cell types. For each method, we measured the average classification accuracy excluding the hold-out group, and the accuracy of assigning unlabeled class to the leave-out group in the query. Among the five methods compared, SCINA, scmap and scID all have metrics scores above the average level of all tools tested (**Figure 4C**). In particular, scmap and SCINA have the 1st and 2nd best-ranked accuracies persistently.

However, SCINA has better accuracy in rejecting cell groups existing in the query dataset but not in the reference (**Figure 4D**). The caveat here, however, is that none of the rejection-enabled methods are among the best performing methods in terms of overall accuracy, stability and robustness to cell type similarities. Since accuracy, stability and robustness are probably more important attributes to assess these methods, the practical guide value based on the results of unknown population detection is limited.

Time and memory comparison

In order to compare the runtime and memory utilization of the deconvolution methods, we simulated six data sets each composed of 20,000 genes, with 5 cell types of equal proportion (20%), in total cell numbers of 5,000, 10,000, 15,000, 20,000, 25,000, 50,000, respectively (see **Methods**). All methods show increases in computation time and memory usage when the number of cells increases (**Figure 5**). Of the five top-performing methods in the intra-data and inter-data deconvolution evaluations (**Figure 1**), singleCellNet and CP outperform others on speed (**Figure 5A**). As the dataset size increases beyond 50,000 cells, methods such RPC require a runtime as large as 6 hours. For memory utilization, singleCellNet and CP consistently require less memory than other top performing methods (**Figure 5B**). Notably, the best performing method Seurat (by accuracy) requires memories as large as 100GB, when dataset size increases beyond 50,000 cells, which is significantly larger than most other methods. In all, based on computation speed and memory efficiency, singleCellNet and CP outperform others among the top-class accurate deconvolution methods.

Discussion

In this study, we presented comprehensive evaluations of 10 computational deconvolution methods in R packages, on single cell RNA-Seq data. Of the 10 methods, 8 of them are designed for single-cell RNA-seq data, and 2 of them are our unique adaptation from methylation-based analysis. We evaluated these methods on 6 publicly available scRNA-seq datasets as well as several additional simulation datasets. We systematically assessed accuracy (through intra-dataset and inter-dataset predictions), the robustness of each method with challenges from gene filtering, cell-types with high similarity and the capabilities on rare population detection and unknown population detection. In summary, we found that methods such as Seurat, SingleR, CP, RPC and

SingleCellNet performed well overall, with Seurat being the best-performing methods in annotating major cell types. Methods such as Seurat, SingleR and CP are more robust against down-sampling. However, Seurat does have a major drawback at predicting rare cell populations, as well as minor issues at differentiating highly similar cell types, while SingleR and CP are much better in these aspects.

During the preparation of the manuscript, another evaluation paper was published in a special edition of Genome Biology [22]. We, therefore, address the similarity and difference between these two studies' methodologies, before discussing our own findings in detail. For computational methods, we only selected the packages in R, as R is still the most popular bioinformatics platform for open-source scRNA-Seq analysis packages (e.g. the arguably most popular method Seurat, which the other study omitted). Also, we uniquely introduced and modified two methods: Linear Constrained Projection (CP) and Robust Partial Correlations (RPC). Although they were originally developed for DNA methylation data deconvolution, their regression-based principle could be adapted to scRNA-seq deconvolution. We modified the final regression coefficients as the probability of one specific cell type label, rather than the cell content as in DNA methylation-based deconvolution. As the results indicated, CP has comparable prediction with SingleR, the overall second best method. This shows the potential of repurposing existing deconvolution methods from another omics analysis. For benchmark datasets, we used fewer real experimental datasets. However, we uniquely included many simulated datasets while the other study did not use any. We argue that it is important to have additional simulation datasets, because evaluation based on manually annotated cell-type-specific markers in the experimental data is prone to bias. On the contrary, one can introduce simulation datasets with 'ground truth' and unbiasedly assess the tricky issues, such as identifying highly similar cell populations or very rare cell populations. We do think, however, that the simulations may overly simplify the complexity of single cells in the heterogeneous tissue, and further methodological development is needed to generate simulation datasets better mimicking real data.

The high deconvolution performance of Seurat on intra-data and inter-data predictions in our study, is mostly due to the fact that it's an integration method which aligns the query and reference dataset using Canonical Correlation Analysis (CCA). CCA captures the correlated source of variation between datasets, and Seurat uses L2 normalization to correct the scales, followed by the

mutual nearest neighbors algorithm to define anchor pairs across datasets. Therefore, the batch-correcting and data integrating features from Seurat contribute to its good overall performance. Although having slightly lower accuracy metrics scores, SingleR and CP still have very excellent performance in overall accuracies, with resilience towards gene filtering and increased complexity in datasets. In addition, SingleR has better performance than Seurat in predicting rare cell populations, as well as differentiating highly similar cell types. This advantage of SingleR may benefit from its method. During the prediction, it uses pseudo-bulk RNA-seq reference to correlate the expression profiles to each of the single cells in the query data, and uses highly variable genes to find the best fit iteratively. For Seurat, the annotation of the cell labels on query data is informed by the nearest anchor pairs. If two or more cell types have similar profiles, their alignments may overlap which may cause misclassification. Seurat also has some requirements on the minimum number of defined anchor pairs. In the case of rare cell populations, the lack of the neighborhood information makes the prediction difficult. Similar to other study [22], we also found that method that incorporates the prior-knowledge (e.g. Garnett and SCINA) did not improve the classification performance over other methods that do not have such requirements. In addition, as the number of cell types increases, the search for the marker genes will become challenging, making these methods even less desirable.

Compared with intra-data prediction, inter-data prediction is more realistic but also more challenging. Technical/platform and batch differences in inter-data prediction may impose major challenges to the classification process, although the tissue and cell type contents are the same. Among all experimental data used as the benchmark in this study, PBMC datasets had the worst accuracy results (ARI=0.76 for the best method Seurat). Further inspection of the confusion matrices revealed that the challenges come from distinguishing highly similar cell types, which themselves may have some level of inaccuracy from the original experiments. If the upstream unsupervised clustering methods are not sensitive enough to categorize similar cell populations, this uncertainty may be carried through to the downstream cell annotation steps. This again highlights the potential issue of evaluating the deconvolution methods, where we are not certain about the ‘ground truth’ of the cell labels to begin with.

Overall, we recommend using Seurat for general deconvolution task for cell types that are relatively separable and without rare population identification as the objective. For datasets contain

cell types with high similarities or rare cell populations, if a reference dataset with clean annotations is available, SingleR and CP are preferable.

Materials and methods

Real data sets

Six real scRNA-seq data sets were downloaded and used for evaluations and validations (**Table 2**). The human pancreatic islet datasets were obtained from the following accession numbers: GEO: GSE85241 (Celseq2) [10,23], GEO: GSE86469 (Fluidigm C1) [10,24]. The *Tabula Muris* datasets Version 2 (10X Genomics and Smart-Seq2) were downloaded from FigShare: https://tabula-muris.ds.czbiohub.org/ [5]. The bead-purified PBMC dataset (10X Genomics) was obtained from the Zheng dataset: https://github.com/10XGenomics/single-cell-3prime-paper, and the PBMC-3K dataset (10X Genomics) was downloaded from https://support.10xgenomics.com/single-cell-gene-expression/datasets [25]. These datasets differ by species, tissue and sequencing protocol. For each of the datasets, we collected both raw counts and cell-type annotations from the corresponding publications, except PBMC-3k, for which the cell-type annotations were obtained through the standard single cell RNA-seq analysis and classified using cell-type-specific marker genes. The extracted cell-type annotations for each dataset were used as the ground truth for evaluations (**Table S1**).

Data cleaning

Datasets were paired in groups by tissue type (**Table 2**). Within a pair, we used sorted, purified dataset as reference data, and the other one as the query data. Both reference data and query data were further processed to make sure the cell types in reference data are larger or equal to the cell types in the query data. When necessary, the query data were down sampled following the original cell type count distribution. For the two Tabula Muris (TM-Full) datasets from 10X and Smart-Seq2 platforms, which contain a large number of cell types (32 and 37 cell types, respectively), we took a subset of cells from lung tissue and created two TM-Lung datasets that have fewer cell types, 8 for 10X and and 10 for Smart-Seq2 platform, respectively. As a result, we have four pairs of experimental datasets: PBMC cell pair with PBMC-sorted-ref and PBMC-3K-query; pancreas cell pair with pancreas-celseq2-ref and pancreas-fluidigm-query; TM-Full pair with TM-Full-

smartseq2-ref and TM-Full-10X-query; TM-Lung pair with TM-Lung-smartseq2-ref and TM-Lung-10x-query.

Data downsampling

To explore the effects of different feature numbers and read depths on the performance of tools, we randomly down sampled features (genes) from human pancreas-Fluidigm dataset into 5000, 10000 and 15000 input genes, following the original log count distribution. We repeated five times for each downsampling scheme. Alternatively, we also down sampled the reads into 25%, 50%, 75% of the original read depths (with 2 repetitions) using *samtools* on BAM files, and then realigned following the method provided by the original manuscript [24].

Simulated Data Sets

We simulated a dataset using Splatter, with 4,000 genes and 2,000 cells (Splatter parameters, dropout.shape=-0.5, dropout.mid=1), and then split each dataset into 5 cell groups with proportions 10%, 30%, 30%, 10% and 20%. In addition, we also generated two additional simulation datasets to evaluate the robustness of tools. In the first set, we generated 10,000 genes and 2,000 cell (use Splatter parameters dropout.shape=-0.5, dropout.mid=1), and then split it into 9 cell groups with proportions 50%, 25%, 12.5%, 6.25%, 3.125%, 1.56%, 0.97%, 0.39%, 0.195%, respectively. The second set contains four simulation datasets, each composed of 10,000 genes and 2,000 cells splitting into 5 cell types with equal proportions. These datasets have the same set of differentially expressed (DE) genes, but differ by the magnitude of DE factors (*de.facScale* parameter in Splatter). The DE scales and the parameterizations are: low: de.facScale = c(0.1, 0.3, 0.1, 0.3, 0.2); low-moderate: de.facScale = c(0.3, 0.5, 0.3, 0.5, 0.4); moderate: de.facScale = c(0.5, 0.7, 0.5, 0.7, 0.6); high: de.facScale = c(0.7, 0.9, 0.7, 0.9, 0.8).

Data Preprocessing

Cell and gene filtering

We filtered out cells for which fewer than 200 genes were detected and any genes that were expressed in fewer than 3 cells.

Normalization

For the deconvolution tools that require a normalized count matrix as input, we performed log-normalization using a size factor of 10,000.

Pseudo-bulk reference matrix

For the deconvolution tools that use bulk rather than single-cell expression profiles as reference, we took the average of the normalized count of each cell type group and made a pseudo-bulk RNA-seq reference.

Marker genes selection

Some deconvolution tools require cell-type specific markers as the input. When such marker information is neither provided by the corresponding tools nor obtainable by public research, we extracted them from the reference data by performing differential expression analysis (Wilcoxon rank sum test by *FindAllMarkers* function from Seurat with parameters only.pos = TRUE, min.pct = 0.25 and logfc.threshold = 0.25). The top 10 ranked marker genes for each cell type were used as the input for the corresponding tools.

Deconvolution Methods

We only considered pre-printed or published methods with detailed documentation on installation and execution. We excluded any methods that required extensive running time, and where we were unable to customize the reference dataset, or random and inconsistent predictions were produced. In the end, ten cell deconvolution methods, publicly available as R packages, were evaluated in this study. This includes eight methods (Seurat, scmap, SingleR, CHETAH, SingleCellNet, scID, Garnett, and SCINA) commonly used to deconvolute scRNA-seq data. In addition, to investigate the potential to repurpose deconvolution methods for other omics analysis, we also included and modified two methods originally designed for bulk DNA methylation that use a different type of algorithms not yet reported in scRNA-seq specific tools: Linear Constrained Projection (CP) and Robust Partial Correlations (RPC).

All parameters were set to default values following the author's recommendations or the respective manuals (**Table 1**). For methods that allow "unknown" assignments (scmap, CHETAH, scID, Garnett, and SCINA), we modified the parameter to force assignments where possible (except for the evaluations where unknown assignments were allowed).

Adaptation of CP and RPC methods for scRNA-Seq analysis

In order to accommodate methylation-based methods for scRNA-seq data, we made some modifications. RPC and CP model the methylation profile of any given single cell sample as a linear combination of a signature matrix of different cell types. In the modified version, we treated the estimated weight for each cell type as probability and the cell type with the highest weight was the identity of the corresponding single cell sample in the query data. We took the subset of pseudo-bulk RNA-seq data by keeping features that exhibited high cell-to-cell variations in the reference dataset and had a small condition number below 3 as the signature matrix. We set the highly variable genes to 2000, using *FindVaraibleFeatures* function from Seurat.

Benchmarking

Five-fold cross validation and cross-dataset prediction

For each dataset in four pairs of the real experimental datasets mentioned above, we used a 5-fold cross validation where the four-fold data were used as the reference and the remaining one-fold as the query. For the cross-dataset prediction, in addition to the four pairs of real datasets, we used simulation datasets containing true assay (without dropouts) as the reference and raw assay (with dropout mask) as the query.

Performance evaluation on the effect of feature numbers and read depths

To investigate the robustness of different methods with regards to feature numbers and read depths, we used the down-sampled human pancreas Fluidigm data set as described in the data downsampling section. In such evaluation, the human pancreas Celseq2 dataset was used as the reference and the down-sampled human pancreas Fluidigm dataset was used as a query.

Performance evaluation with effect of differential expression (DE) scale among cell groups

In this assessment, we used four simulation data sets containing the same DE gene set but differing only by DE factors as described earlier in the Simulated Data Sets section. For each simulation data set, the true assay (without dropouts) was used as the reference and the raw assay (with dropout mask) was used as the query.

Rare and unknown population detection

The simulation data in the rare population detection evaluation was composed of 10, 000 genes and 2,000 cells splitting into 9 cell types with proportions 50%, 25%, 12.5%, 6.25%, 3.125%, 1.56%, 0.97%, 0.39%, 0.195%. The simulation dataset in the unknown population detection evaluation was composed of 4,000 genes and 2,000 cells splitting into 5 cell types. We used the scheme of "hold-out one cell type evaluation" to evaluate prediction on the unknown population, that is, removing the signature of one cell type in the reference matrix while predicting the query. During each prediction, one cell group was removed from the reference matrix and the query remained intact. We repeated the evaluation five times for all five cell types. Similarly, for each simulation data set, the true assay (without dropouts) was used as the reference and the raw assay (with dropout mask) was used as the query.

Runtime and Memory Assessment

In order to compare the computational runtime and memory utilization of deconvolution methods, we simulate six datasets, with total cell numbers of 5,000, 10,000, 15,000, 20,000, 25,000, and 50,000, respectively, each composed of 20,000 genes, splitting into 5 cell types with the equal proportion. The true assay (without dropouts) was used as the reference and the raw assay (with dropout mask) was used as the query. Each execution was performed in a separate R session in our lab server (4 nodes (Dell PowerEdge C6420) of 2 X Intel(R) Xeon(R) Gold 6154 CPU @ 3.00GHz, 192GB RAM, one node (Dell Poweredge R740) with 2 X Xeon(R) Gold 6148 CPU @ 2.40GHz, 192 GB RAM, and two 16GB Nvidia V100 GPUs) with Slurm job scheduler. One processor and 100GB memory were reserved for each job. From the job summary, we collected 'Job Wall-clock time' and 'Memory Utilized' for evaluation. We ran each method on each dataset five times to estimate the average computation time.

Evaluation Criteria

The prediction results of the methods are evaluated using three different metrics: overall accuracy, adjusted rand index, and V-measure. The detailed explanations on these metrics were described earlier [26] [27]. Briefly, *Overall accuracy* is the percent agreement between the predicted label and the true label. *Adjusted rand index* (ARI) is the ratio of all cell pairs that are either correctly classified together or correctly not classified together, among all possible pairs, with adjustment for chance. *V-measure* is computed as the harmonic mean of distinct homogeneity and completeness score. In specific, homogeneity is used to assess whether each predicted cell type

groups contains only members of a single class, while completeness is used to assess whether all members of a given class are assigned to the same predicted cell label.

Code Availability

All the codes and data are available at:
https://github.com/qianhuiSenn/scRNA_cell_deconv_benchmark.

Authors' Contributions

LG, and QH envisioned this project. QH implemented the project and conducted the analysis with help from YL and YD. QH and LG wrote the manuscript. All authors have read and agreed on the manuscript.

Competing interests

The authors declare no competing financial interests.

Acknowledgements

This research was supported by grants K01ES025434 awarded by NIEHS through funds provided by the trans-NIH Big Data to Knowledge (BD2K) initiative (www.bd2k.nih.gov), R01 LM012373 and R01 LM012907 awarded by NLM, R01 HD084633 awarded by NICHD to L.X. Garmire.

References

[1] Cao J, Spielmann M, Qiu X, Huang X, Ibrahim DM, Hill AJ, et al. The single-cell transcriptional landscape of mammalian organogenesis. Nature 2019;566:496–502.

[2] Zhu X, Wolfgruber TK, Tasato A, Arisdakessian C, Garmire DG, Garmire LX. Granatum: a graphical single-cell RNA-Seq analysis pipeline for genomics scientists. Genome Med 2017;9:108.

[3] Zhu X, Yunits B, Wolfgruber T, Poirion O, Arisdakessian C, Garmire L. GranatumX: A community engaging and flexible software environment for single-cell analysis. bioRxiv 2018:385591. doi:10.1101/385591.

[4] Plass M, Solana J, Wolf FA, Ayoub S, Misios A, Glažar P, et al. Cell type atlas and lineage tree of a whole complex animal by single-cell transcriptomics. Science 2018;360. doi:10.1126/science.aaq1723.

[5] Tabula Muris Consortium, Overall coordination, Logistical coordination, Organ collection and processing, Library preparation and sequencing, Computational data analysis, et al.

Single-cell transcriptomics of 20 mouse organs creates a Tabula Muris. Nature 2018;562:367–72.
[6] Zappia L, Phipson B, Oshlack A. Exploring the single-cell RNA-seq analysis landscape with the scRNA-tools database. PLoS Comput Biol 2018;14:e1006245.
[7] Bacher R, Kendziorski C. Design and computational analysis of single-cell RNA-sequencing experiments. Genome Biol 2016;17:63.
[8] Rostom R, Svensson V, Teichmann SA, Kar G. Computational approaches for interpreting scRNA-seq data. FEBS Lett 2017;591:2213–25.
[9] Poirion OB, Zhu X, Ching T, Garmire L. Single-Cell Transcriptomics Bioinformatics and Computational Challenges. Front Genet 2016;7:163.
[10] Stuart T, Butler A, Hoffman P, Hafemeister C, Papalexi E, Mauck WM 3rd, et al. Comprehensive Integration of Single-Cell Data. Cell 2019;177:1888–902.e21.
[11] Kiselev VY, Yiu A, Hemberg M. scmap: projection of single-cell RNA-seq data across data sets. Nat Methods 2018;15:359–62.
[12] Aran D, Looney AP, Liu L, Wu E, Fong V, Hsu A, et al. Reference-based analysis of lung single-cell sequencing reveals a transitional profibrotic macrophage. Nat Immunol 2019;20:163–72.
[13] de Kanter JK, Lijnzaad P, Candelli T, Margaritis T, Holstege FCP. CHETAH: a selective, hierarchical cell type identification method for single-cell RNA sequencing. Nucleic Acids Res 2019. doi:10.1093/nar/gkz543.
[14] Tan Y, Cahan P. SingleCellNet: A Computational Tool to Classify Single Cell RNA-Seq Data Across Platforms and Across Species. Cell Syst 2019;9:207–13.e2.
[15] Boufea K, Seth S, Batada NN. scID: Identification of transcriptionally equivalent cell populations across single cell RNA-seq data using discriminant analysis. bioRxiv 2019:470203. doi:10.1101/470203.
[16] Pliner HA, Shendure J, Trapnell C. Supervised classification enables rapid annotation of cell atlases. Nat Methods 2019;16:983–6.
[17] Zhang Z, Luo D, Zhong X, Choi JH, Ma Y, Wang S, et al. SCINA: Semi-Supervised Analysis of Single Cells in silico. Genes 2019;10:531.
[18] Teschendorff AE, Breeze CE, Zheng SC, Beck S. A comparison of reference-based algorithms for correcting cell-type heterogeneity in Epigenome-Wide Association Studies. BMC Bioinformatics 2017;18:105.
[19] Rand WM. Objective Criteria for the Evaluation of Clustering Methods. J Am Stat Assoc 1971;66:846–50.
[20] Rosenberg A, Hirschberg J. V-measure: A conditional entropy-based external cluster evaluation measure. Proceedings of the 2007 joint conference on empirical methods in natural language processing and computational natural language learning (EMNLP-CoNLL), 2007, p. 410–20.
[21] Zappia L, Phipson B, Oshlack A. Splatter: simulation of single-cell RNA sequencing data. Genome Biol 2017;18:174.
[22] Abdelaal T, Michielsen L, Cats D, Hoogduin D, Mei H, Reinders MJT, et al. A comparison of automatic cell identification methods for single-cell RNA sequencing data. Genome Biology 2019;20. doi:10.1186/s13059-019-1795-z.
[23] Muraro MJ, Dharmadhikari G, Grün D, Groen N, Dielen T, Jansen E, et al. A Single-Cell Transcriptome Atlas of the Human Pancreas. Cell Syst 2016;3:385–94.e3.
[24] Lawlor N, George J, Bolisetty M, Kursawe R. Single-cell transcriptomes identify human

islet cell signatures and reveal cell-type–specific expression changes in type 2 diabetes. Genome 2017.
[25] Zheng GXY, Terry JM, Belgrader P, Ryvkin P, Bent ZW, Wilson R, et al. Massively parallel digital transcriptional profiling of single cells. Nat Commun 2017;8:14049.
[26] Arisdakessian C, Poirion O, Yunits B, Zhu X, Garmire LX. DeepImpute: an accurate, fast, and scalable deep neural network method to impute single-cell RNA-seq data. Genome Biol 2019;20:211.
[27] Poirion O, Zhu X, Ching T, Garmire LX. Using single nucleotide variations in single-cell RNA-seq to identify subpopulations and genotype-phenotype linkage. Nat Commun 2018;9:4892.

Figure Legends

Figure 1. Accuracy comparison among methods using eight experimental scRNA-seq datasets and one pair of simulated scRNA-seq datasets

(A-C) Within data accuracy comparison, shown as heatmaps of three classification metrics, (**A**) overall accuracy, (**B**) adjusted rand index, and (**C**) v-measure across eight real datasets. For each dataset, a 5-fold cross validation is performed: using four folds as the reference and one-fold as the query. **(D-F)** Between-data accuracy comparison, shown as heatmaps of three classification metrics, (**D**) overall accuracy, (**E**) adjusted rand index, and (**F**) v-measure across four pairs of experimental datasets and one pair of simulation datasets. PBMC cell pair: PBMC-sorted-ref and PBMC-3K-query; pancreas pair: pancreas-celseq2-ref and pancreas-fluidigm-query; TM-Full pair: TM-Full-smartseq2-ref and TM-Full-10X-query; TM-Lung pair: TM-Lung-smartseq2-ref and TM-Lung-10x-query; simulation: true-ref and dropout-masked raw. TM-Lung datasets pair was down sampled from TM-Full datasets pair by taking cells from lung tissue only. Within the simulation datasets pair, the true assay without dropouts (true-ref) was used as the reference and the raw assay with dropout mask (raw-query) was used as the query. The columns are datasets, and the rows are deconvolution methods. The heatmap scale is shown on the figure, where the brighter yellow color indicates a better classification accuracy score. On the right of each heatmap is a boxplot to summarize the classification metrics among methods. Box colors represent different methods as shown in the figure. The methods in the heatmap and the boxplot are arranged in descending order by their average metrics score across all datasets. Some methods failed to produce a prediction for certain data sets (indicated by grey squares).

****: significantly higher ($P<0.05$) than 9 other methods using pairwise Wilcoxon test.

***: significantly higher (P<0.05) than 8 other methods using pairwise Wilcoxon test.

**: significantly higher (P<0.05) than 7 other methods using pairwise Wilcoxon test.

*: significantly higher (P<0.05) than 6 other methods using pairwise Wilcoxon test.

Figure 2. Effect of differential gene expression scale among cell groups on deconvolution tool performance

(A) PCA plots of four sets of simulation datasets generated by Splatter, each of which is composed of 10,000 genes and 2,000 cells, splitting into 5 cell types with equal proportion, and contains the same proportion of differentially expressed genes in each cell type. The datasets differ by changing the magnitude of DE factors for those DE genes to simulate more or less differences between groups. Based on the magnitude of DE factors in five cell groups, we generated four datasets with cell groups similarity ranging from low, low-moderate, moderate to high DE (see **Methods**). Colors represent different cell types. True assay (without dropouts) is used as the query and raw assay (with dropout) is used as the reference. **(B-D)** Plots showing three classification metrics to evaluate each deconvolution method applied to the four datasets in (**A**). The x-axis is the DE scale for differential expressed genes in each group, and the y-axis is the metric score. Line colors and point shapes correspond to different methods. The metrics are: (**B**) overall accuracy, (**C**) adjusted rand index and (**D**) v-measure.

Figure 3. Effects of feature (gene) numbers and read depths on the performance of deconvolution methods

(A) The features (genes) in the human pancreas-fluidigm dataset are filtered by removing genes that present in less than 3 cells, resulting in 19211 genes. The filtered features (genes) are randomly down sampled into 5000, 10000 and 15000 input genes, following the original log count distribution. Such down-sampling was repeated 5 times. **(C)** The BAM file reads in the human pancreas-fluidigm dataset are randomly down sampled into 25%, 50%, 75% of the original read depths. **(B)(D)** Plots depicting the three classification metrics (overall accuracy, adjusted rand index and v-measure) of each method applied to the down sampling approaches in (**A**) and (**C**) respectively. The x-axis is the down sampling size for feature numbers or reads, and the y-axis is

the metrics score. Line colors and point shapes correspond to different methods. SCINA failed when the number of input features reached 5000, thus no point is shown.

Figure 4. Performance comparison on rare cell type and unknown cell types detection among the deconvolution methods

All datasets are generated by Splatter. **(A)** Cell population distribution of simulation data, composed of 10,000 genes and 2,000 cells, split into 9 cell types with proportions of 50%, 25%, 12.5%, 6.25%, 3.125%, 1.56%, 0.97%, 0.39%, 0.195%, respectively. **(B)** Plot illustrating cell-type specific accuracy across 9 cell groups in (**A**), for deconvolution methods that exceed 0.8 in overall accuracy and adjusted rand index. The x-axis is the cell groups in the descending order for their cell proportions, and the y-axis is the cell-type specific classification score. **(C)** Performance metrics (overall accuracy, adjusted rand index and v-measure) of another simulation data set, composed of 4,000 genes and 2,000 cells splitting into 5 cell types. True assay (without dropouts) is used as the reference and the raw assay (with dropout) is used as the query. During each prediction, one cell group is removed from the reference matrix and the query remains intact. The x-axis lists methods with rejection options (e.g. allowing 'unlabeled' samples), and the y-axis is the classification metrics score excluding the hold-out -group. **(D)** Boxplots showing the accuracy of the top 2 methods in (**C**), when assigning 'unlabeled' class to the leave-out group in the query.

Figure 5. Speed and memory usage comparison among deconvolution tools

Speed and memory comparison on six pairs of simulation data with increasing numbers of cells (5000, 10000, 15000, 20000, 25000, 50000). True assay (without dropouts) is used as the reference and the raw assay (with dropout) is used as the query. Both reference and query contain the same number of cells. Color depicts different deconvolution methods. **(A)** Natural log of running time (y-axis) vs. cell size (x-axis) over five repetitions in each data point. **(B)** Natural log of peak memory usage (y-axis) vs. cell size (x-axis) over five repetitions in each data point.

Tables

Table 1. List of Single-Cell RNA-sequencing/Methylation Cell Deconvolution tools benchmarked in this study. The tools are compared with respect to their algorithms and characteristics

Table 2. Datasets used in this study

Supplementary material

Supplementary Figures

Supplementary Figure 1

Illustration of the workflow for this study consists of 1) preprocessing 2) prediction 3) evaluations

Supplementary Figure 2. The optimal number of highly variable genes (HVG) to be used in CP and RPC algorithms

The highly variable genes are identified from reference dataset and ranked by standardized variance from mean-variance feature selection methods with variance-stabilizing transformation. **(A)** The boxplot depicts the overall accuracy averaged over five pairs of inter-dataset predictions (pbmc, pancreas, tabula-Full, tabula-Lung, and simulation) with the top 100, 200, 500, 1000, 2000, and 5000 highly variable genes as input features for CP and RPC methods. The x-axis is the number of highly variable features, and the y-axis is the overall accuracy. Methods are reflected by different box colors. **(B)** The boxplot represents the condition number of the pseudo-bulk reference matrix averaged over four combinations of cross-dataset predictions with the top 100, 200, 500, 1000, 2000, and 5000 highly variable genes as input features. The x-axis is the number of highly variable features, and the y-axis is the condition number.

Supplementary Figure 3-7

Confusion matrix of cell-type specific accuracy for each of the four combinations of cross-dataset predictions among top-5-performing deconvolution methods. The x-axis is the predicted label from each algorithm and the y-axis is the true label in the query data.

Supplementary Tables

Supplementary Table 1. Composition of cell-types in each real dataset.

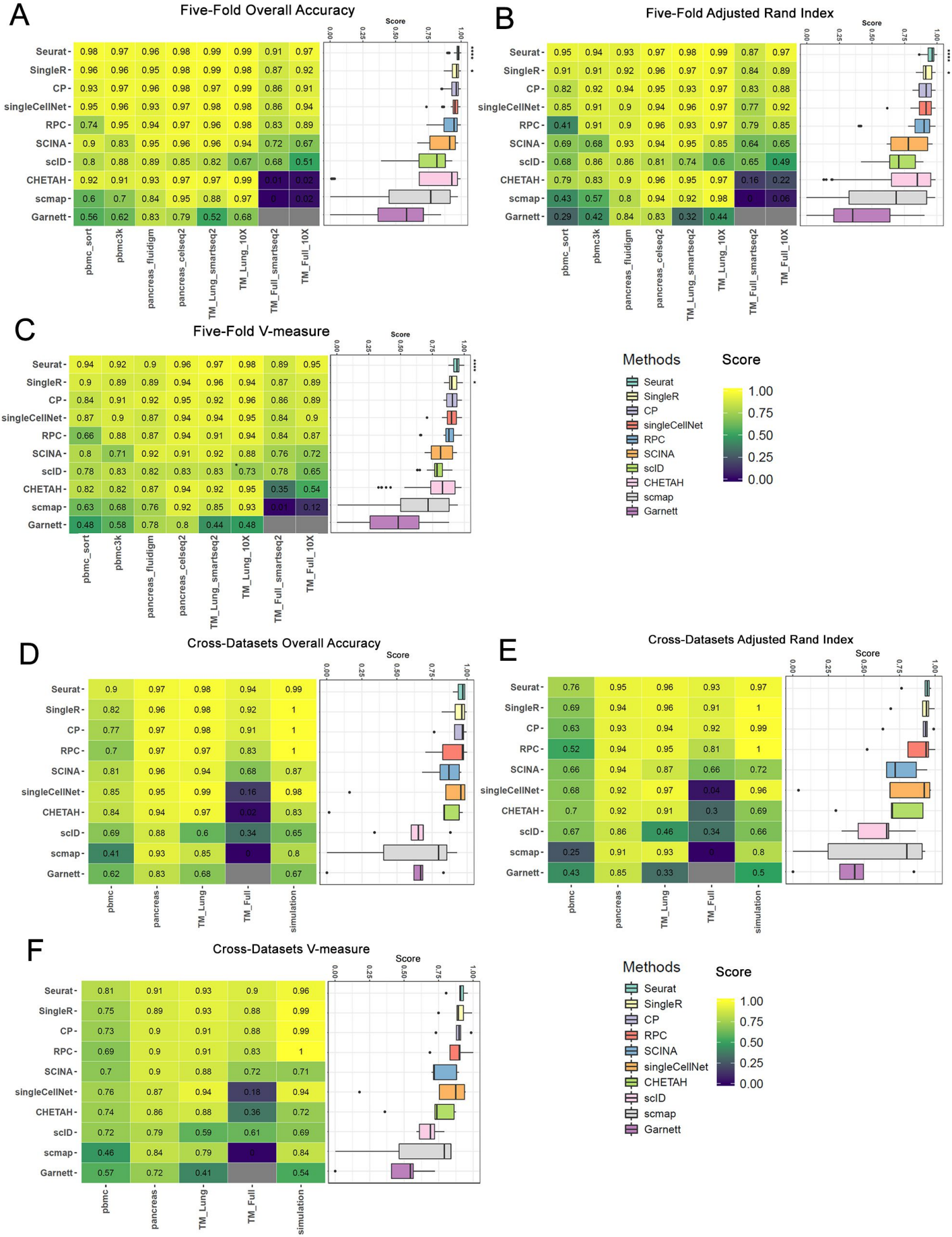
A
Five-Fold Overall Accuracy
Score
Seurat 0.98 0.97 0.96 0.98 0.99 0.99 0.91 0.97
SingleR 0.96 0.96 0.95 0.98 0.99 0.98 0.87 0.92
CP 0.93 0.97 0.96 0.98 0.97 0.99 0.86 0.91
singleCellNet 0.95 0.96 0.93 0.97 0.98 0.98 0.86 0.94
RPC 0.74 0.95 0.94 0.97 0.96 0.98 0.83 0.89
SCINA 0.9 0.83 0.95 0.96 0.96 0.94 0.72 0.67
scID 0.8 0.88 0.89 0.85 0.82 0.67 0.68 0.51
CHETAH 0.92 0.91 0.93 0.97 0.97 0.99 0.01 0.02
scmap 0.6 0.7 0.84 0.95 0.88 0.97 0 0.02
Garnett 0.56 0.62 0.83 0.79 0.52 0.68
pbmc_sort
pbmc3k
pancreas_fluidigm
pancreas_celseq2
TM_Lung_smartseq2
TM_Lung_10X
TM_Full_smartseq2
TM_Full_10X
B
Five-Fold Adjusted Rand Index
Score
Seurat 0.95 0.94 0.93 0.97 0.98 0.99 0.87 0.97
SingleR 0.91 0.91 0.92 0.96 0.97 0.97 0.84 0.89
CP 0.82 0.92 0.94 0.95 0.93 0.97 0.83 0.88
singleCellNet 0.85 0.91 0.9 0.94 0.96 0.97 0.77 0.92
RPC 0.41 0.91 0.9 0.96 0.93 0.97 0.79 0.85
SCINA 0.69 0.68 0.93 0.94 0.95 0.85 0.64 0.65
scID 0.68 0.86 0.86 0.81 0.74 0.6 0.65 0.49
CHETAH 0.79 0.83 0.9 0.96 0.95 0.97 0.16 0.22
scmap 0.43 0.57 0.8 0.94 0.92 0.98 0 0.06
Garnett 0.29 0.42 0.84 0.83 0.32 0.44
pbmc_sort
pbmc3k
pancreas_fluidigm
pancreas_celseq2
TM_Lung_smartseq2
TM_Lung_10X
TM_Full_smartseq2
TM_Full_10X
C
Five-Fold V-measure
Score
Seurat 0.94 0.92 0.9 0.96 0.97 0.98 0.89 0.95
SingleR 0.9 0.89 0.89 0.94 0.96 0.94 0.87 0.89
CP 0.84 0.91 0.92 0.95 0.92 0.96 0.86 0.89
singleCellNet 0.87 0.9 0.87 0.94 0.94 0.95 0.84 0.9
RPC 0.66 0.88 0.87 0.94 0.91 0.94 0.84 0.87
SCINA 0.8 0.71 0.92 0.91 0.92 0.88 0.76 0.72
scID 0.78 0.83 0.82 0.83 0.83 0.73 0.78 0.65
CHETAH 0.82 0.82 0.87 0.94 0.92 0.95 0.35 0.54
scmap 0.63 0.68 0.76 0.92 0.85 0.93 0.01 0.12
Garnett 0.48 0.58 0.78 0.8 0.44 0.48
pbmc_sort
pbmc3k
pancreas_fluidigm
pancreas_celseq2
TM_Lung_smartseq2
TM_Lung_10X
TM_Full_smartseq2
TM_Full_10X
Methods
Seurat
SingleR
CP
singleCellNet
RPC
SCINA
scID
CHETAH
scmap
Garnett
Score
1.00
0.75
0.50
0.25
0.00
D
Cross-Datasets Overall Accuracy
Score
Seurat 0.9 0.97 0.98 0.94 0.99
SingleR 0.82 0.96 0.98 0.92 1
CP 0.77 0.97 0.98 0.91 1
RPC 0.7 0.97 0.97 0.83 1
SCINA 0.81 0.96 0.94 0.68 0.87
singleCellNet 0.85 0.95 0.99 0.16 0.98
CHETAH 0.84 0.94 0.97 0.02 0.83
scID 0.69 0.88 0.6 0.34 0.65
scmap 0.41 0.93 0.85 0 0.8
Garnett 0.62 0.83 0.68 0.67
pbmc
pancreas
TM_Lung
TM_Full
simulation
E
Cross-Datasets Adjusted Rand Index
Score
Seurat 0.76 0.95 0.96 0.93 0.97
SingleR 0.69 0.94 0.96 0.91 1
CP 0.63 0.93 0.94 0.92 0.99
RPC 0.52 0.94 0.95 0.81 1
SCINA 0.66 0.94 0.87 0.66 0.72
singleCellNet 0.68 0.92 0.97 0.04 0.96
CHETAH 0.7 0.92 0.91 0.3 0.69
scID 0.67 0.86 0.46 0.34 0.66
scmap 0.25 0.91 0.93 0 0.8
Garnett 0.43 0.85 0.33 0.5
pbmc
pancreas
TM_Lung
TM_Full
simulation
F
Cross-Datasets V-measure
Score
Seurat 0.81 0.91 0.93 0.9 0.96
SingleR 0.75 0.89 0.93 0.88 0.99
CP 0.73 0.9 0.91 0.88 0.99
RPC 0.69 0.9 0.91 0.83 1
SCINA 0.7 0.9 0.88 0.72 0.71
singleCellNet 0.76 0.87 0.94 0.18 0.94
CHETAH 0.74 0.86 0.88 0.36 0.72
scID 0.72 0.79 0.59 0.61 0.69
scmap 0.46 0.84 0.79 0 0.84
Garnett 0.57 0.72 0.41 0.54
pbmc
pancreas
TM_Lung
TM_Full
simulation
Methods
Seurat
SingleR
CP
RPC
SCINA
singleCellNet
CHETAH
scID
scmap
Garnett
Score
1.00
0.75
0.50
0.25
0.00

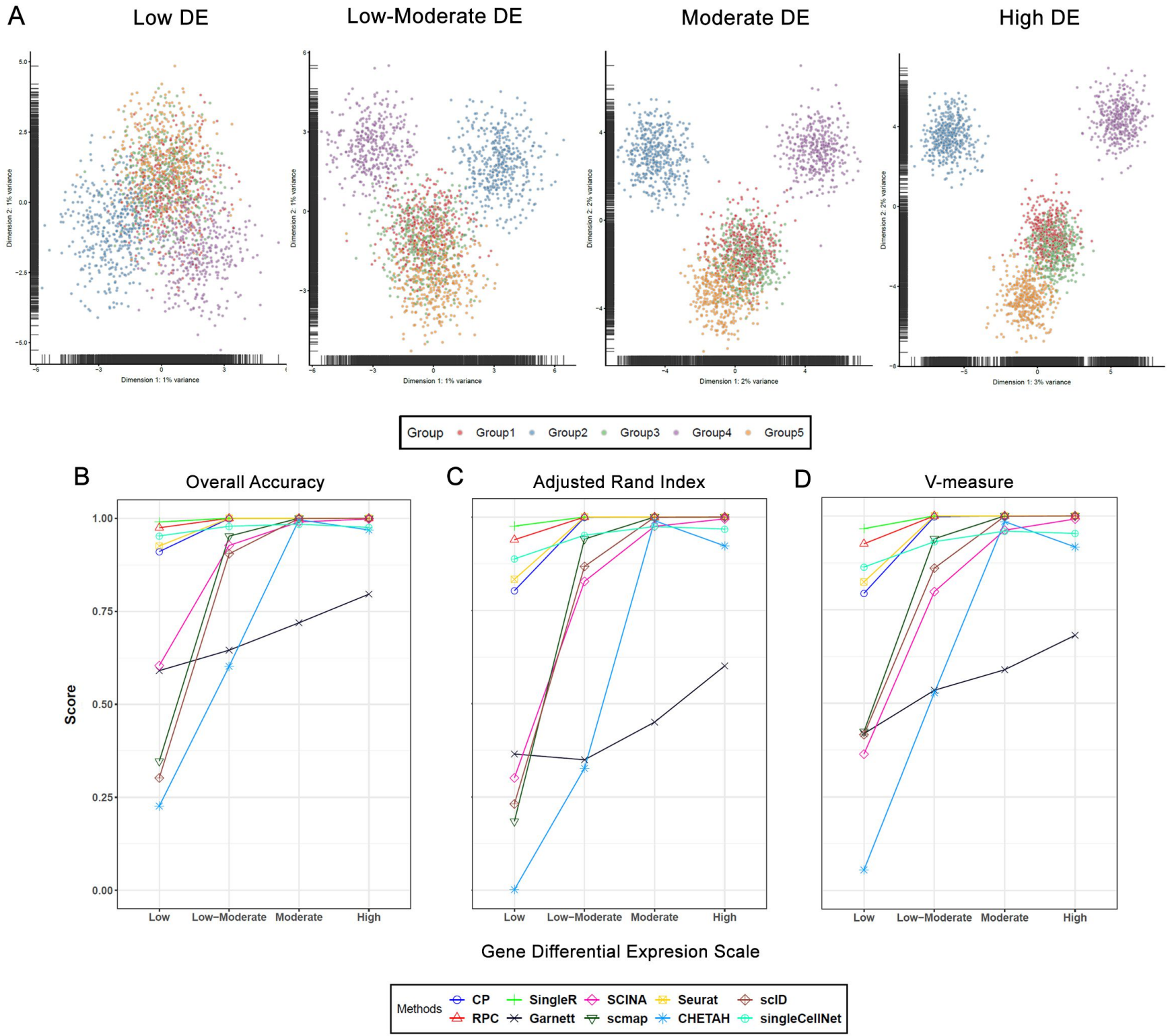
A
Low DE
Low-Moderate DE
Moderate DE
High DE
Dimension 1: 1% variance
Dimension 2: 1% variance
Dimension 1: 2% variance
Dimension 2: 2% variance
Dimension 1: 3% variance
Group
Group1
Group2
Group3
Group4
Group5
B
Overall Accuracy
C
Adjusted Rand Index
D
V-measure
Score
Low
Low−Moderate
Moderate
High
Gene Differential Expresion Scale
Methods
CP
SingleR
SCINA
Seurat
scID
RPC
Garnett
scmap
CHETAH
singleCellNet

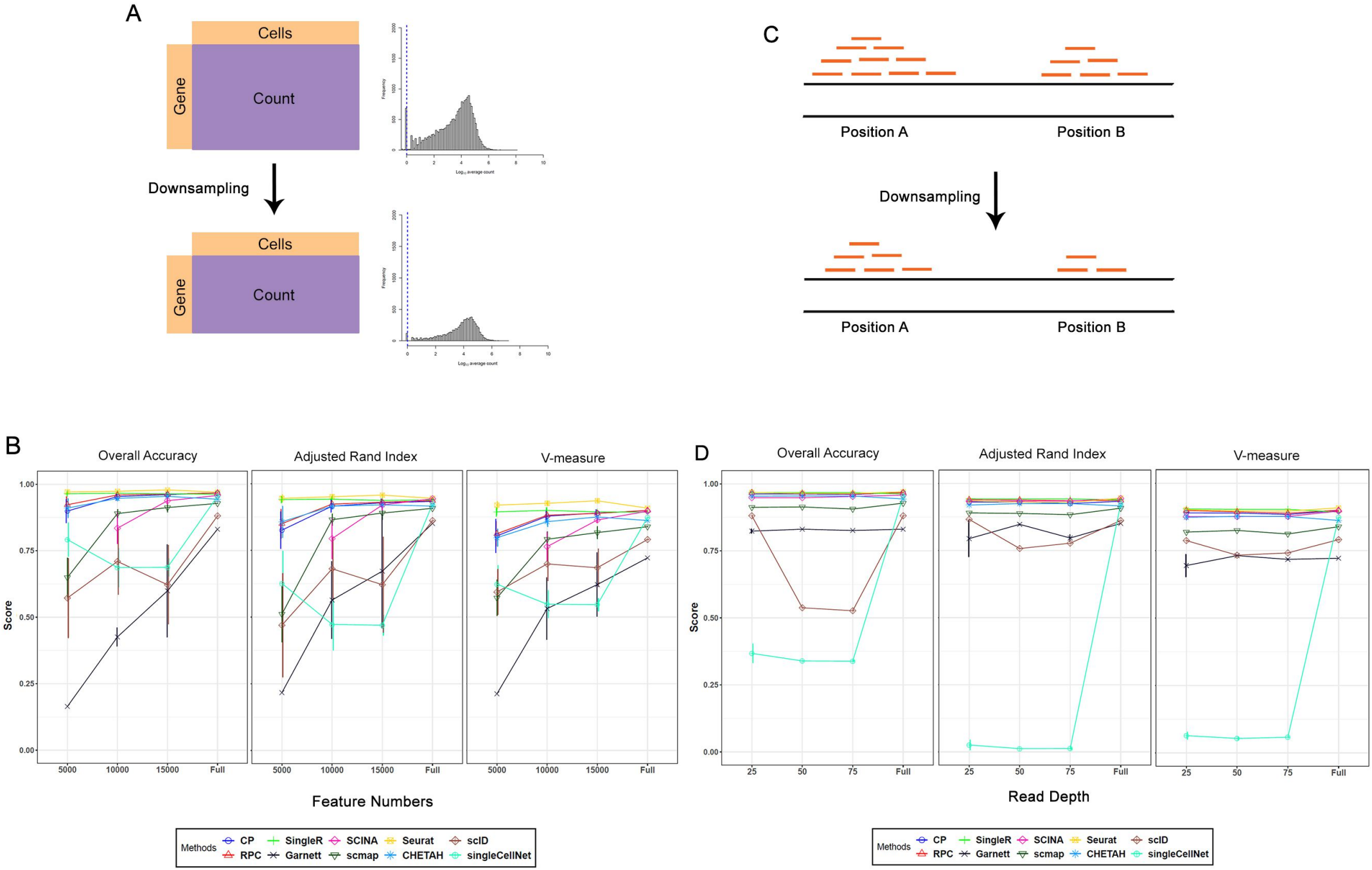
A
Cells
Gene
Count
Downsampling
Cells
Gene
Count
C
Position A
Position B
Downsampling
Position A
Position B
B
Overall Accuracy
Adjusted Rand Index
V-measure
Score
Feature Numbers
5000
10000
15000
Full
D
Overall Accuracy
Adjusted Rand Index
V-measure
Score
Read Depth
25
50
75
Full
Methods
CP
SingleR
SCINA
Seurat
scID
RPC
Garnett
scmap
CHETAH
singleCellNet

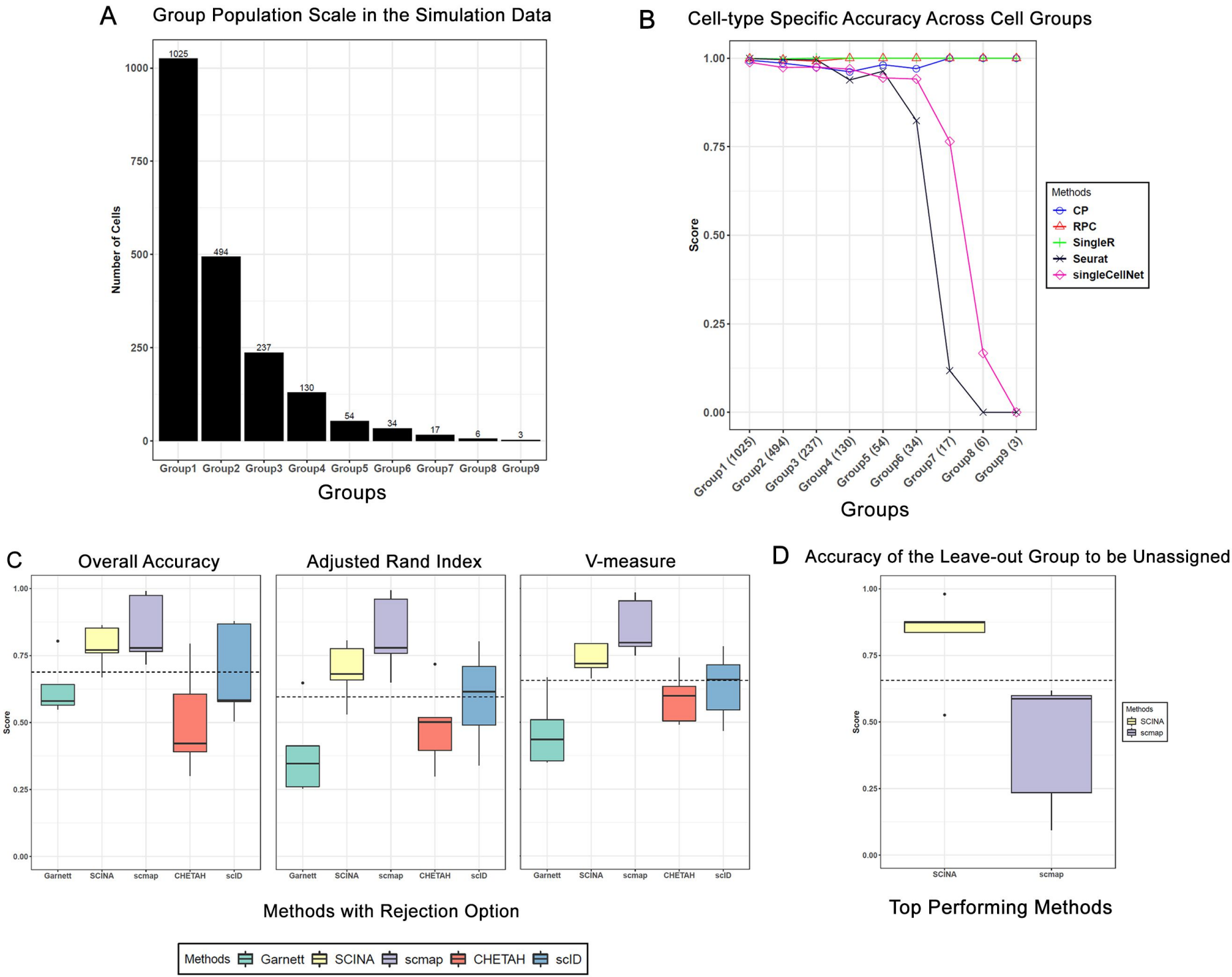
A
Group Population Scale in the Simulation Data
Number of Cells
1025
494
237
130
54
34
17
6
3
Group1 Group2 Group3 Group4 Group5 Group6 Group7 Group8 Group9
Groups
B
Cell-type Specific Accuracy Across Cell Groups
Score
Methods
CP
RPC
SingleR
Seurat
singleCellNet
Group1 (1025)
Group2 (494)
Group3 (237)
Group4 (130)
Group5 (54)
Group6 (34)
Group7 (17)
Group8 (6)
Group9 (3)
Groups
C
Overall Accuracy
Adjusted Rand Index
V-measure
Score
Garnett SCINA scmap CHETAH scID
Methods with Rejection Option
Methods Garnett SCINA scmap CHETAH scID
D
Accuracy of the Leave-out Group to be Unassigned
Score
Methods
SCINA
scmap
SCINA scmap
Top Performing Methods

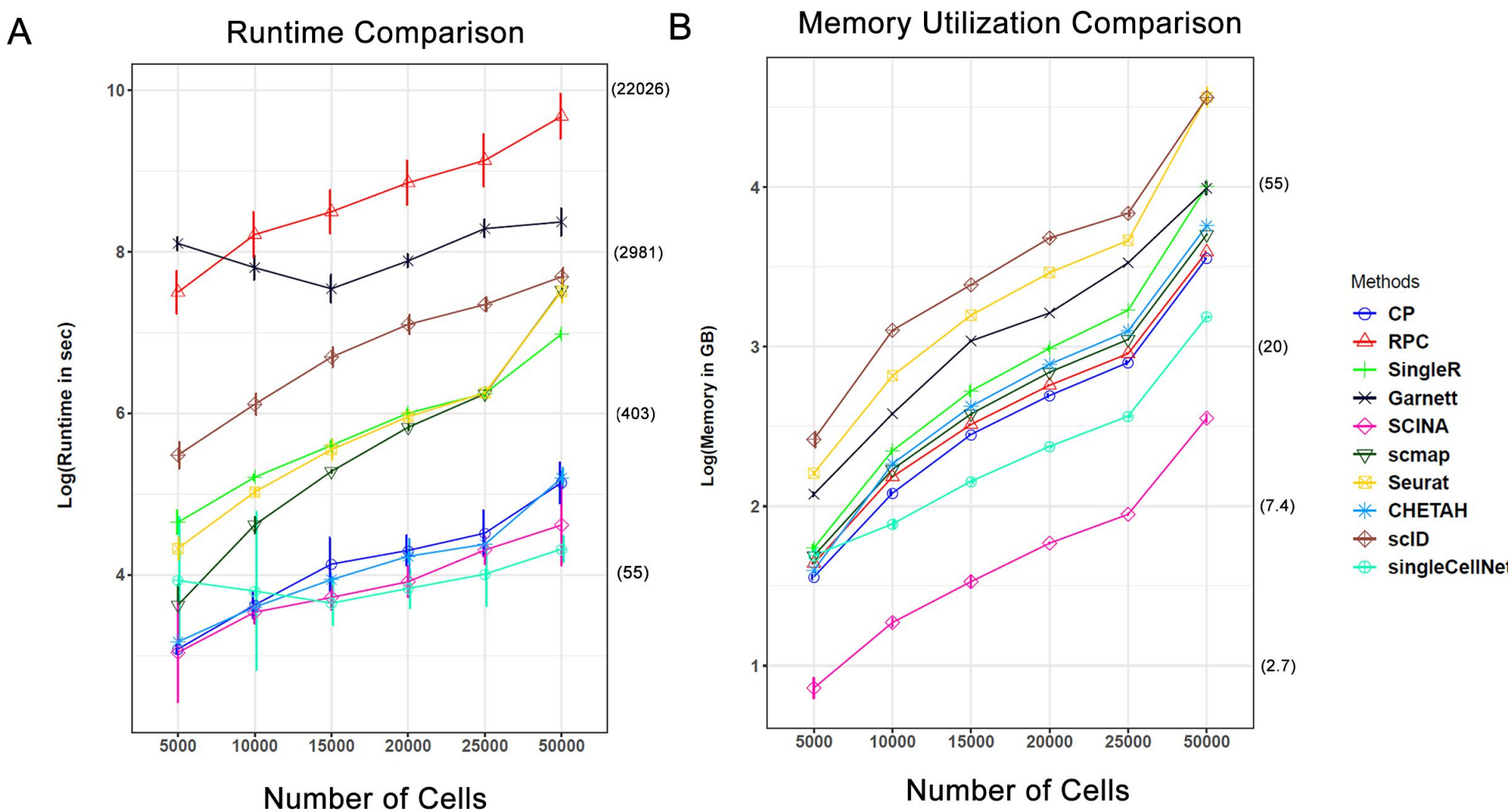
A
Runtime Comparison
Log(Runtime in sec)
10
8
6
4
(22026)
(2981)
(403)
(55)
5000
10000
15000
20000
25000
50000
Number of Cells
B
Memory Utilization Comparison
Log(Memory in GB)
4
3
2
1
(55)
(20)
(7.4)
(2.7)
5000
10000
15000
20000
25000
50000
Number of Cells
Methods
CP
RPC
SingleR
Garnett
SCINA
scmap
Seurat
CHETAH
scID
singleCellNet

Table 1 List of Single-Cell RNA-sequencing/Methylation Cell Deconvolution tools benchmarked in this study. The tools are compared with respect to their algorithms and characteristics

Software	Method/Algorithm	Bulk/Single Reference	Require Pre-defined Marker Genes	Allow Unknown	Version Under R 3.6.0	Reference
SingleR	Correlation-based with Iterative Tuning	Bulk	No	No	SingleR_1.0.0	[9]
CP	Reference-based method using Constrained Projection	Bulk	No	No	EpiDISH_2.0.2	[15]
RPC	Reference-based Robust Partial Correlations	Bulk	No	No	EpiDISH_2.0.2	[15]
Garnett	Elastic net Multinomial Regression	Single	Yes	Yes	garnett_0.1.4	[13]
SCINA	Bimodal Distribution assumption for marker genes	Single	Yes	Yes	SCINA_1.1.0	[14]
Seurat	Define anchor with CCA, L2-norm and MNN	Single	No	No	Seurat_3.0.1	[7]
singleCellNet	Multi-Class Random Forest	Single	No	No	singleCellNet_0.1.0	[11]
CHETAH	Correlation-based with Hierarchical Classification	Single	No	Yes	CHETAH_1.1.2	[10]
scmap	K-nearest-neighbor classification with cosine similarity	Single	No	Yes	scmap_1.6.0	[8]
scID[a]	Fisher's Linear Discriminant Analysis-like Framework	Single	No	Yes	scID_0.0.0.9000	[12]

[a]Methods are published in preprint.

Table 2 Datasets used in this study

Dataset Name	Protocol	No. of Cells	No. of Genes	No. of Cell Types	Species/Tissue/ Description	Reference
PBMC-Sorted	10X	91,649	18,986	7	Human Peripheral Blood Mononuclear Cells	[22]
PBMC-3K	10X	2,467	13,714	6	Human Peripheral Blood Mononuclear Cells	10X Genomics
Pancreas-Sorted	CEL-Seq2	2,285	34,363	13	Human Pancreas	[20] [7]
Pancreas	Fluidigm C1	638	34,363	13	Human Pancreas	[21] [7]
Tabula Muris-Sorted	Smart-Seq2	24,622	22,252	37	Mouse	[2]
Tabula Muris	10X	20,000	17,866	32	Mouse	[2]
Tabula Muris Lung-Sorted	Smart-Seq2	1,563	22,253	10	Mouse Lung	[2]

Tabula Muris Lung	10X	1,303	17,866	8	Mouse Lung	[2]
Simulation1_true	Splatter	2,000	4,000	5	Simulation data for inter-data prediction	
Simulation1_raw[a]	Splatter	2,000	4,000	5	N/A	
Simulation2_true	Splatter	2,000	10,000	9	Simulation data with descending cell proportion for each cell group	
Simulation2_raw[a]	Splatter	2,000	10,000	9	N/A	
Simulation_Low_true	Splatter	2,000	10,000	5	Simulation data with low differential expression scale for each cell group	
Simulation_Low_raw[a]	Splatter	2,000	10,000	5	N/A	
Simulation_Low_Moderate_true	Splatter	2,000	10,000	5	Simulation data with low-moderate differential expression scale for each cell group	
Simulation_Low_Moderate_raw[a]	Splatter	2,000	10,000	5	N/A	
Simulation_Moderate_true	Splatter	2,000	10,000	5	Simulation data with moderate differential expression scale for each cell group	

Simulation_Moderate_raw[a]	Splatter	2,000	10,000	5	N/A
Simulation_High_true	Splatter	2,000	10,000	5	Simulation data with high differential expression scale for each cell group
Simulation_High_raw[a]	Splatter	2,000	10,000	5	N/A

[a] Raw data is true simulation data with the addition of dropouts.

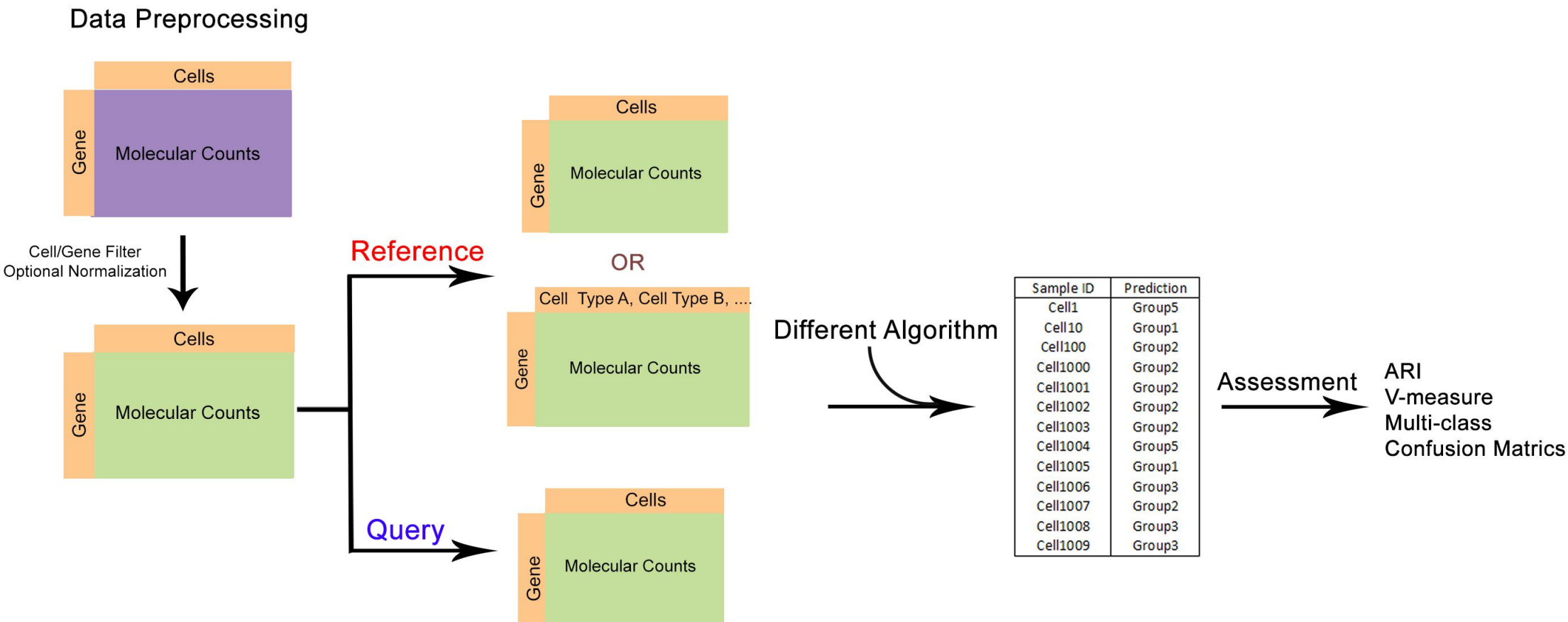
Data Preprocessing
Cells
Gene
Molecular Counts
Cell/Gene Filter
Optional Normalization
Cells
Gene
Molecular Counts
Reference
Query
Cells
Gene
Molecular Counts
OR
Cell Type A, Cell Type B, ...
Gene
Molecular Counts
Cells
Gene
Molecular Counts
Different Algorithm
Sample ID | Prediction
Cell1 | Group5
Cell10 | Group1
Cell100 | Group2
Cell1000 | Group2
Cell1001 | Group2
Cell1002 | Group2
Cell1003 | Group2
Cell1004 | Group5
Cell1005 | Group1
Cell1006 | Group3
Cell1007 | Group2
Cell1008 | Group3
Cell1009 | Group3
Assessment
ARI
V-measure
Multi-class
Confusion Matrics

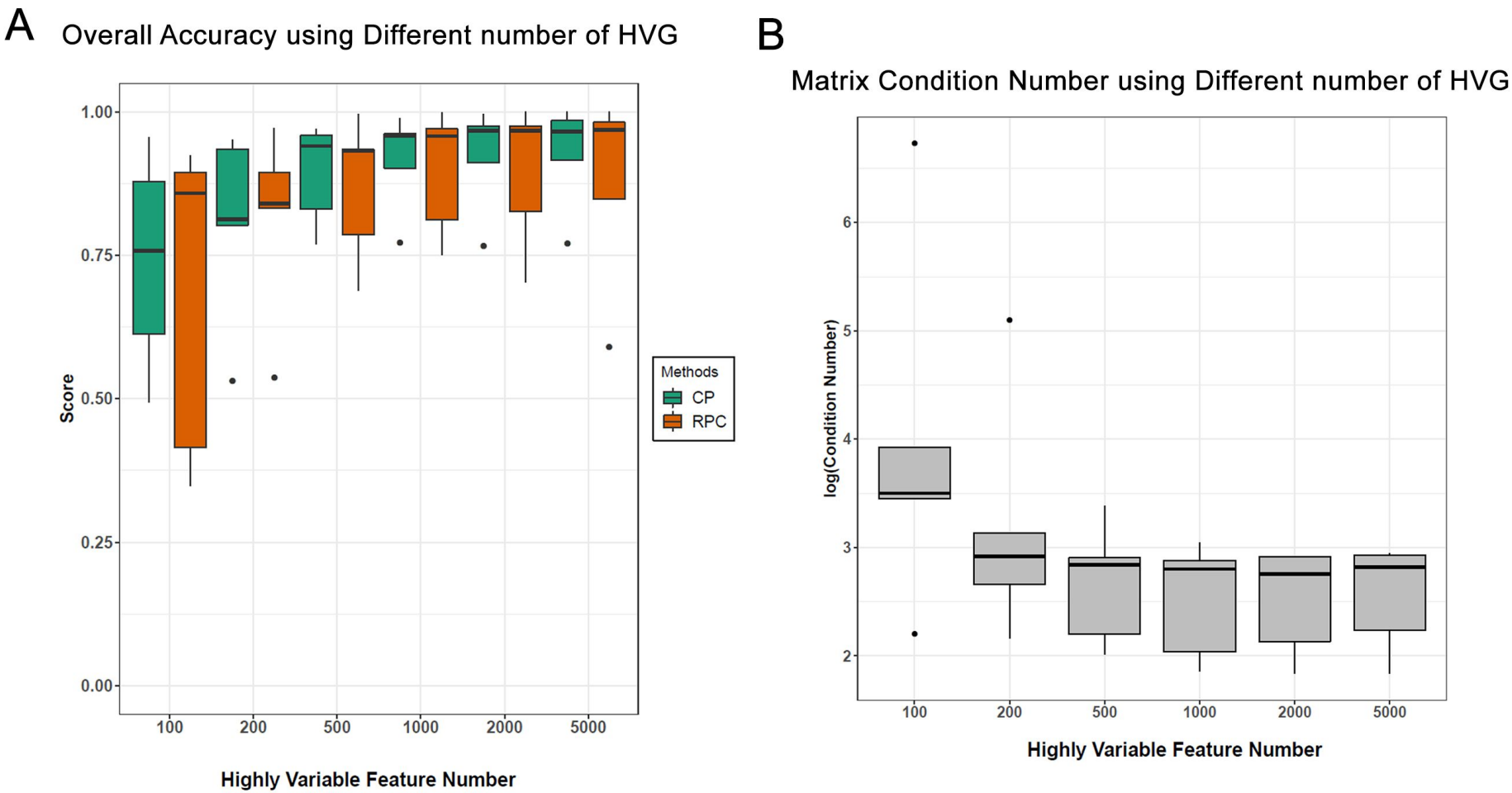
A
Overall Accuracy using Different number of HVG
Score
1.00
0.75
0.50
0.25
0.00
100
200
500
1000
2000
5000
Highly Variable Feature Number
Methods
CP
RPC
B
Matrix Condition Number using Different number of HVG
log(Condition Number)
6
5
4
3
2
100
200
500
1000
2000
5000
Highly Variable Feature Number

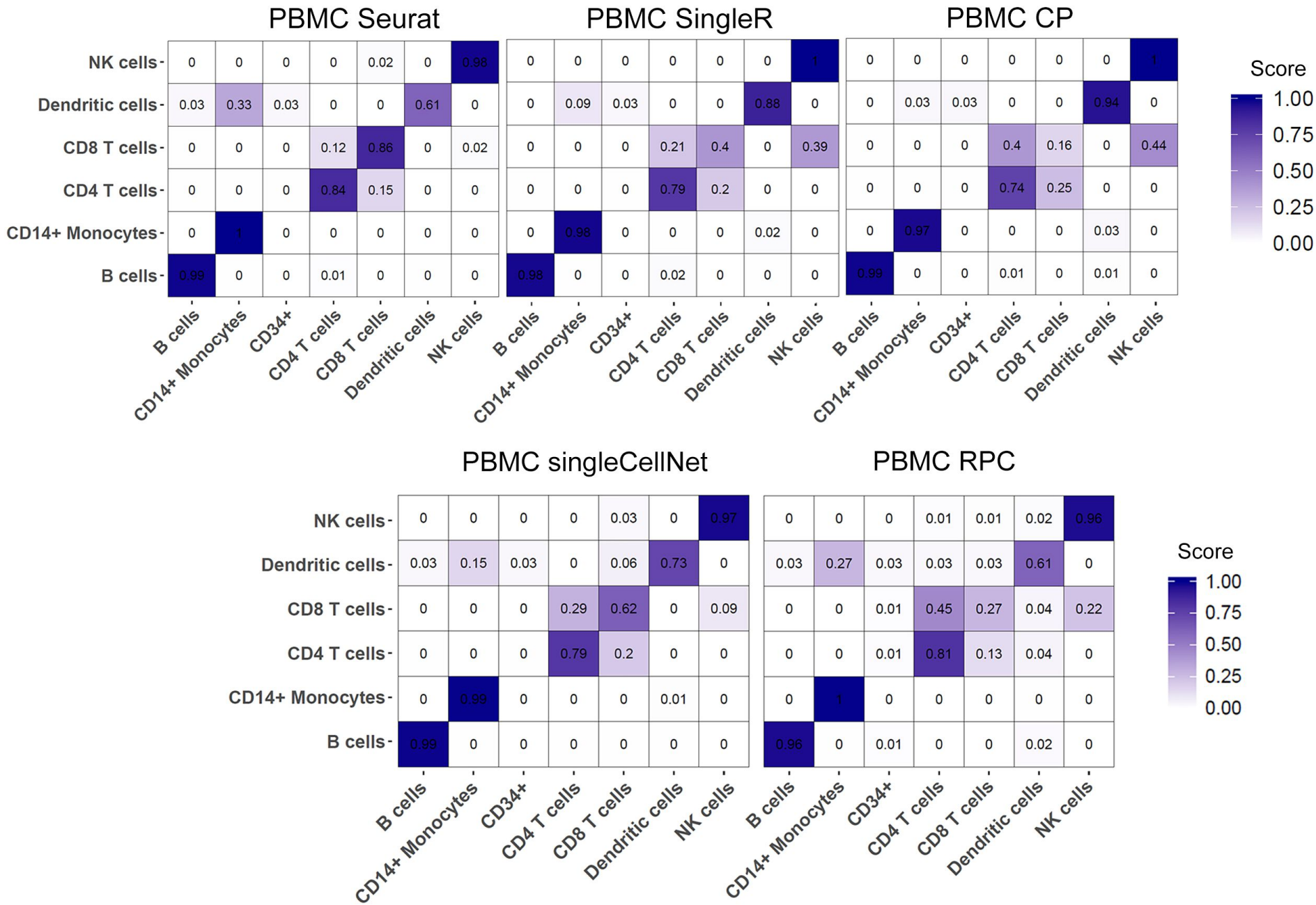
PBMC Seurat
PBMC SingleR
PBMC CP
PBMC singleCellNet
PBMC RPC
NK cells
Dendritic cells
CD8 T cells
CD4 T cells
CD14+ Monocytes
B cells
CD34+
Score
1.00
0.75
0.50
0.25
0.00

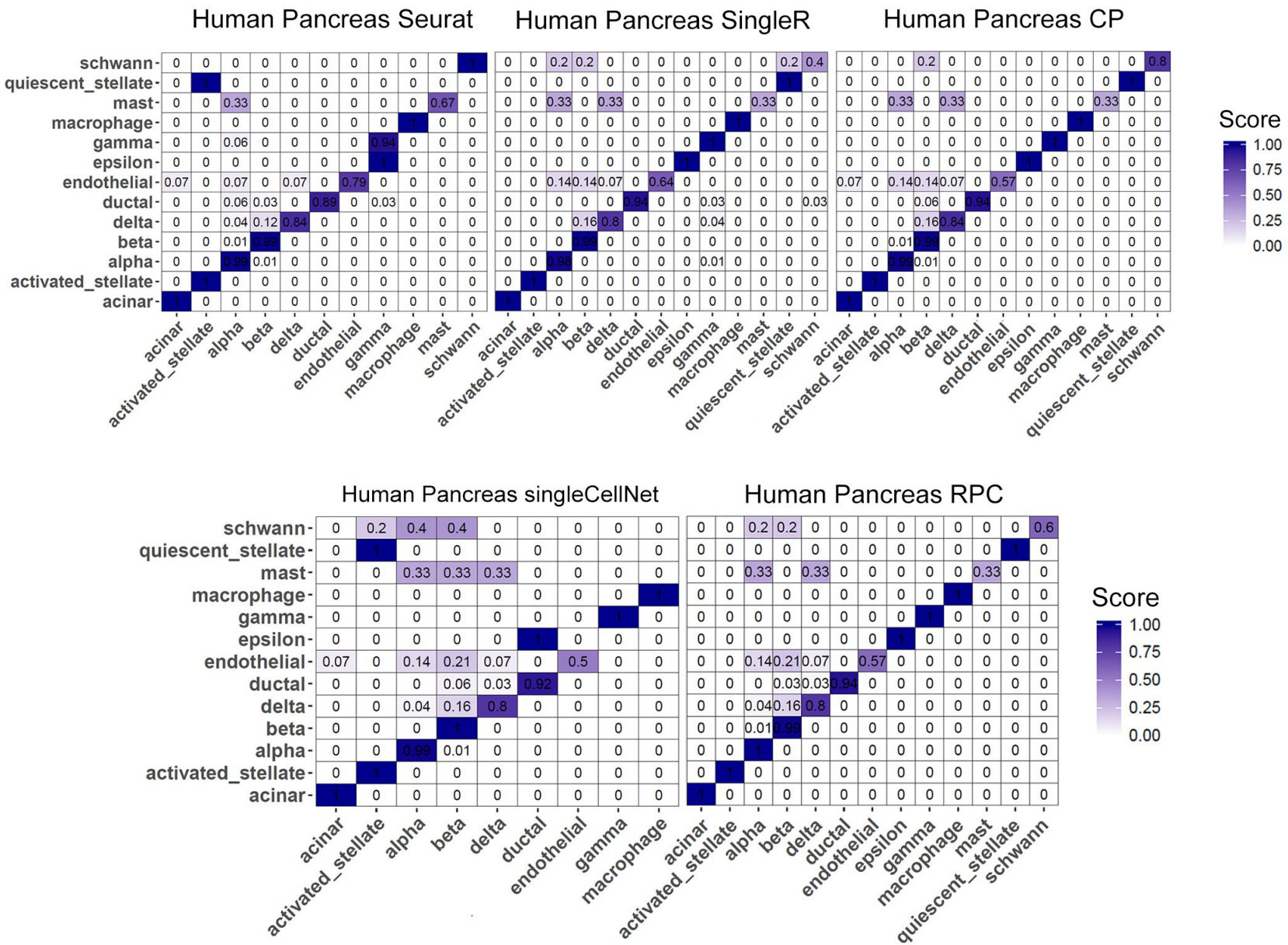
Human Pancreas Seurat
Human Pancreas SingleR
Human Pancreas CP
Human Pancreas singleCellNet
Human Pancreas RPC
schwann
quiescent_stellate
mast
macrophage
gamma
epsilon
endothelial
ductal
delta
beta
alpha
activated_stellate
acinar
Score
1.00
0.75
0.50
0.25
0.00

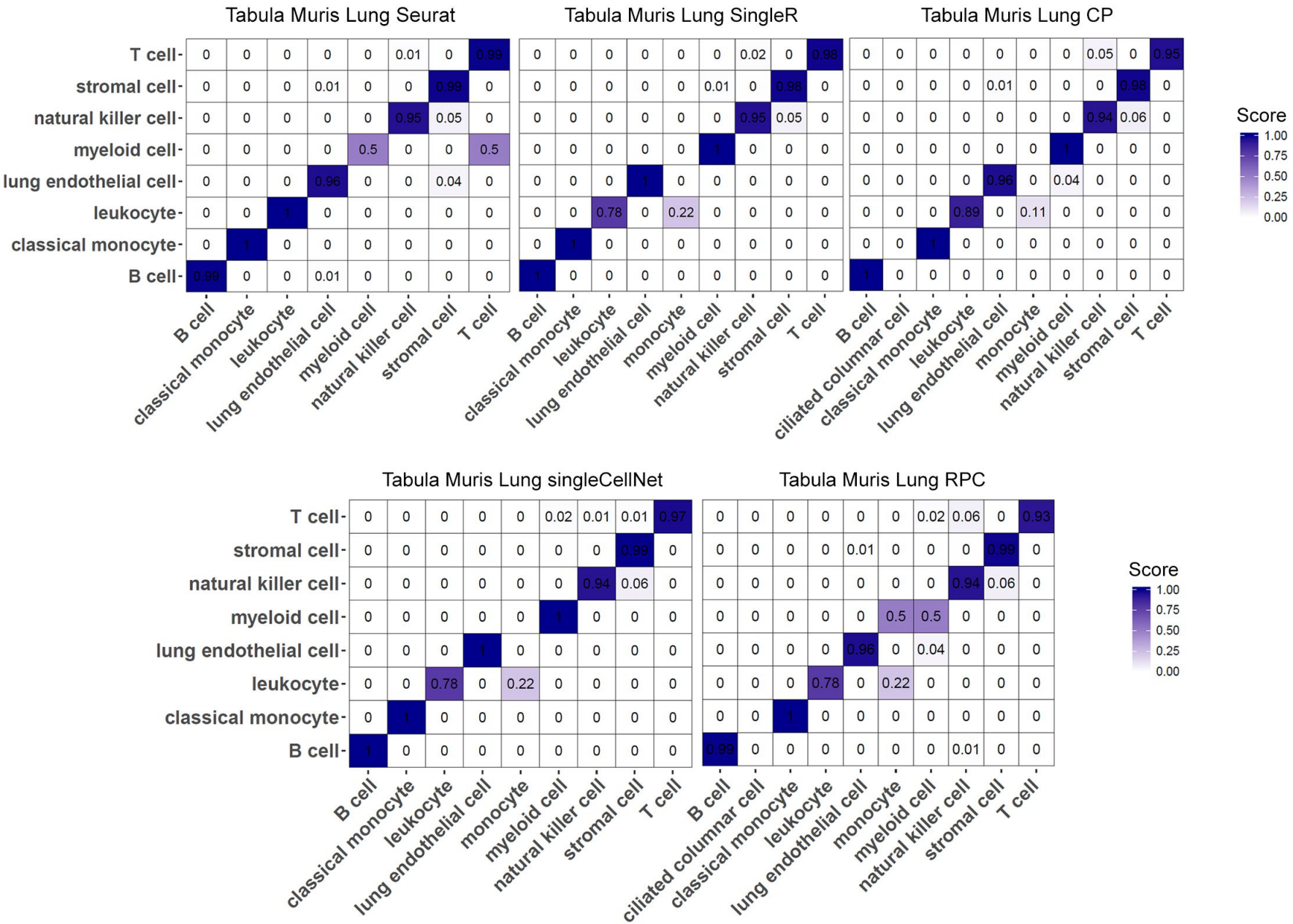
Tabula Muris Lung Seurat
T cell
stromal cell
natural killer cell
myeloid cell
lung endothelial cell
leukocyte
classical monocyte
B cell
B cell
classical monocyte
leukocyte
lung endothelial cell
myeloid cell
natural killer cell
stromal cell
T cell
Tabula Muris Lung SingleR
B cell
classical monocyte
leukocyte
lung endothelial cell
monocyte
myeloid cell
natural killer cell
stromal cell
T cell
Tabula Muris Lung CP
B cell
ciliated columnar cell
classical monocyte
leukocyte
lung endothelial cell
monocyte
myeloid cell
natural killer cell
stromal cell
T cell
Score
1.00
0.75
0.50
0.25
0.00
Tabula Muris Lung singleCellNet
Tabula Muris Lung RPC
Score
1.00
0.75
0.50
0.25
0.00

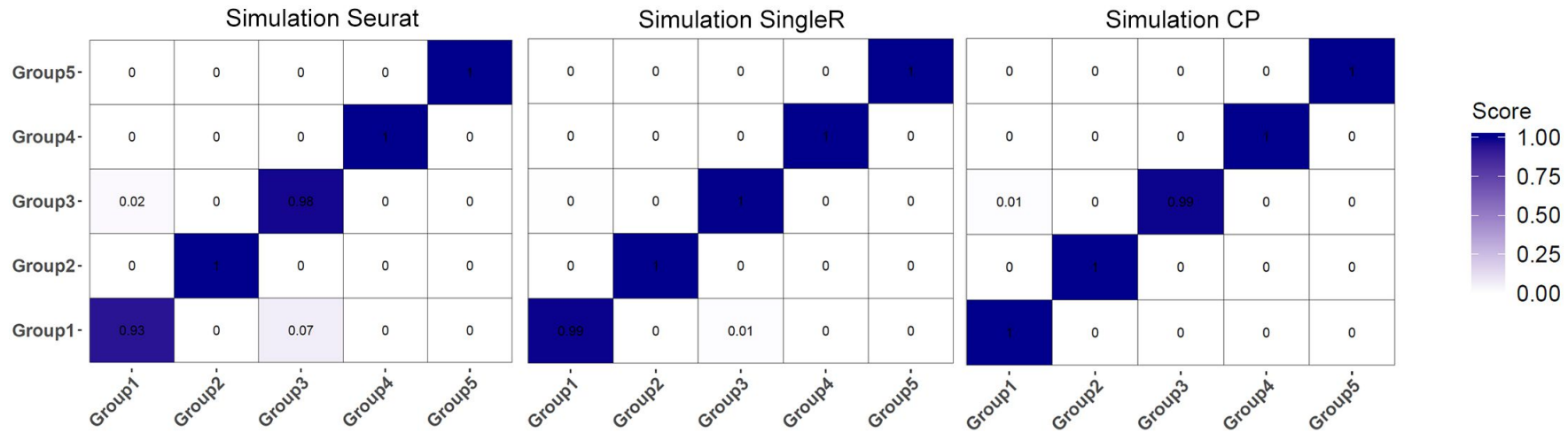
Simulation Seurat
Simulation SingleR
Simulation CP
Group5
Group4
Group3
Group2
Group1
Score
1.00
0.75
0.50
0.25
0.00

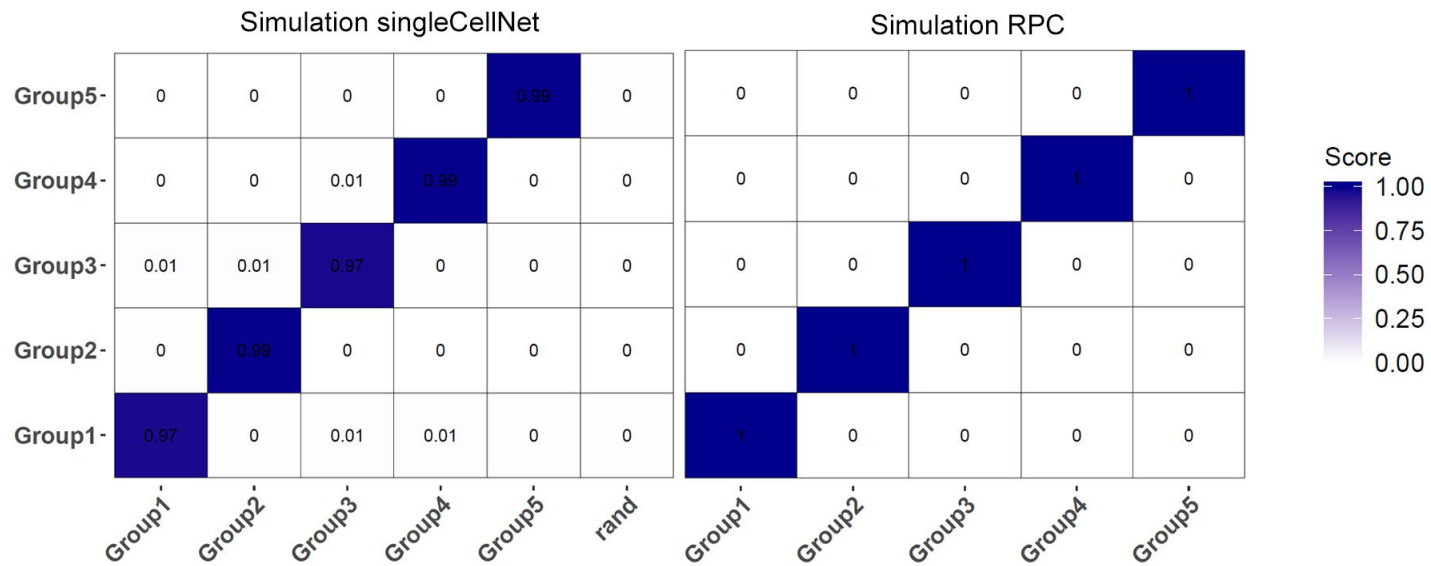
Simulation singleCellNet
Simulation RPC
Group5
Group4
Group3
Group2
Group1
rand
Score
1.00
0.75
0.50
0.25
0.00

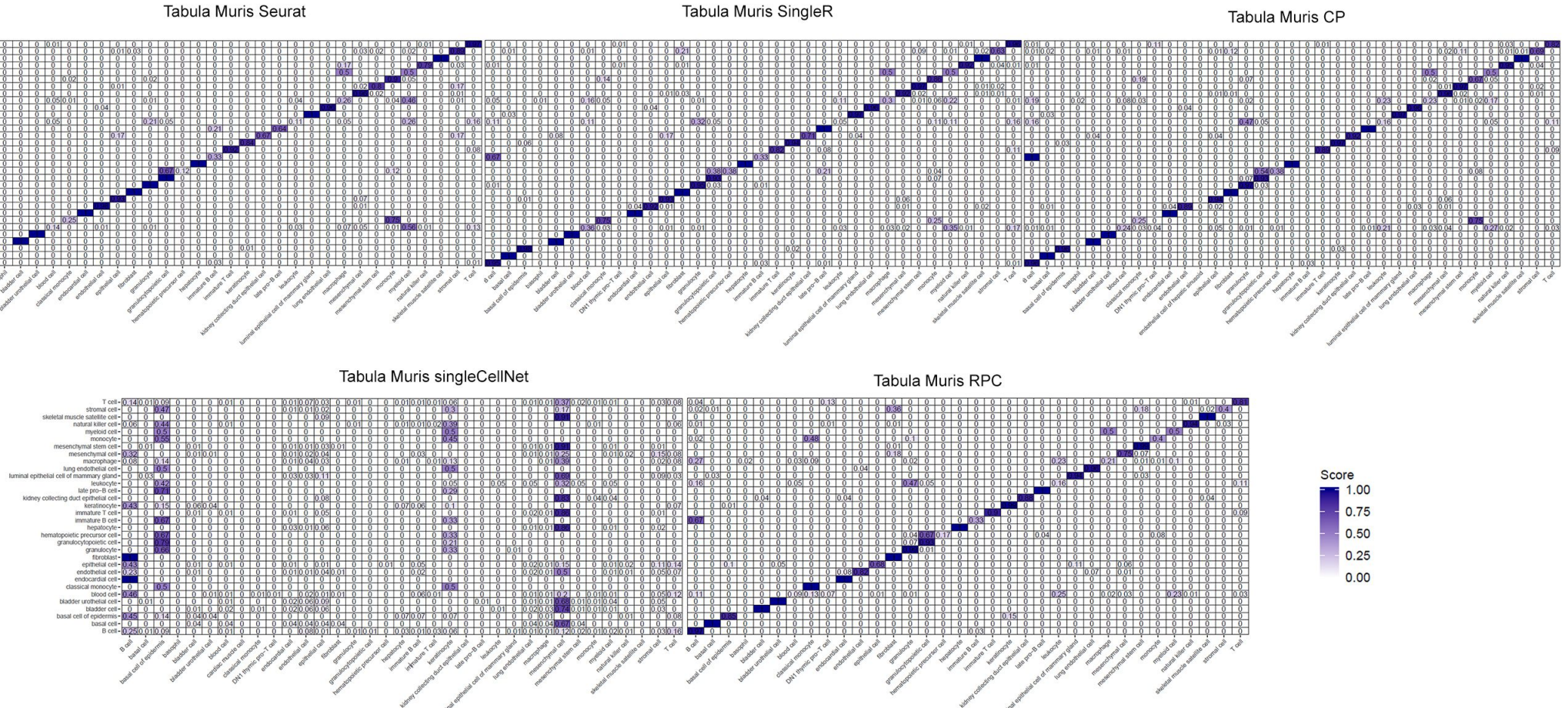
Tabula Muris Seurat
Tabula Muris SingleR
Tabula Muris CP
Tabula Muris singleCellNet
Tabula Muris RPC
Score
1.00
0.75
0.50
0.25
0.00

Supplementary Table 1 Composition of cell-types in each real dataset

	PBMC-Sorted	PBMC-3K	Pancreas--celseq2	Pancreas-Fluidigm	Tabula Muris-Lung-smartseq2	Tabula Muris-Lung-10X	Tabula Muris-Full-smartseq2	Tabula Muris-Full-10X
	B cells (10,084)	B cells (342)	Acinar (274)	Acinar (21)	B cells (57)	B cells (140)	B cells (2029)	B cells (5615)
	CD14+ Monocytes (2,465)	CD14+ Monocytes (2,465)	Activated stella (90)	Activated stella (16)	Cilliated columnar cell (25)		Basal cell (1340)	Basal cell (27)
	CD34+ (6,312)		Alpha (843)	Alpha (239)	Classical monocyte (90)	Classical monocyte (4)	Basal cell of epidermis (1648)	Basal cell of epidermis (2020)
	CD4+ T cells (42,166)	CD4+ T cells (479)	Beta (445)	Beta (258)	Leukocyte (35)	Leukocyte (9)	Basophil (25)	
	CD8+ T cells (22,138)	CD8+ T cells (308)	Delta (203)	Delta (25)	Lung endothelia cell (693)	Lung endothelia cell (24)	Bladder cell (695)	Bladder cell (192)

Cell Type (Cell numbers)	Dendritic cells (99)	Dendritic cells (33)	Ductal (258)	Ductal (36)	Monocyte (65)		Bladder urothelial cell (683)	Bladder urothelial cell (141)
	NK cells (8,385)	NK cells (155)	Endothelial (21)	Endothelial (14)	Myeloid cell (85)	Myeloid cell (2)	Blood cell (206)	Blood cell (153)
			Epsilon (4)	Epsilon (1)	Natural killer cell (37)	Natural killer cell (113)	Cardiac muscle cell (133)	
			Gamma (110)	Gamma (18)	Stromal cell (423)	Stromal cell (888)	Cilliated columnar cell (25)	
			Macrophage (15)	Macrophage (1)	T cell (53)	T cell (123)	Classical monocyte (90)	Classical monocyte (4)
			Mast (6)	Mast (3)			DN1 thymic pro-T cell (32)	

		Quiescent stella (12)	Quiescent stella (1)	Endocardial cell (165)	Endocardial cell (1)
		Schwann (4)	Schwann (5)	Endothelial cell (3319)	Endothelial cell (971)
				Endothelial cell of hepatic sinusoid (182)	
				Epithelial cell (201)	Epithelial cell (99)
				Fibroblast (2189)	Fibroblast (4)
				Granulocyte (761)	Granulocyte (73)

	Granulocytopoietic cell (221)	Granulocytopoietic cell (14)
	Hematopoietic precursor cell (265)	Hematopoietic precursor cell (24)
	Hepatocyte (391)	Hepatocyte (374)
	Immature B cell (344)	Immature B cell (3)
	Immature T cell (1337)	Immature T cell (222)
	Keratinocyte (330)	Keratinocyte (1035)

	Kidney collecting duct epithelial cell (121)	Kidney collecting duct epithelial cell (24)
	Late pro-B cell (306)	Late pro-B cell (14)
	Leukocyte (683)	Leukocyte (19)
	Luminal epithelial cell of mammary gland (578)	Luminal epithelial cell of mammary gland (35)
	Lung endothelial cell (693)	Lung endothelial cell (24)

	Macrophage (395)	Macrophage (208)
	Mesenchymal cell (830)	Mesenchymal cell (5200)
	Mesenchymal stem cell (499)	Mesenchymal stem cell (169)
	Monocyte (331)	Monocyte (42)
	Myeloid cell (1208)	Myeloid cell (2)
	Natural killer cell (171)	Natural killer cell (142)
	Skeletal muscle satellite cell	Skeletal muscle satellite cell (11)

		(540)	
		Stromal cell (863)	Stromal cell (1153)
		T cell (793)	T cell (1985)